Predicting the onset of lithium plating by the full-cell voltage: A pseudo-P curve approach

Ying Kung, Yu-Hong Zhang, Kuo-Ching Chen*, Chih-Hung Chen, Chi-Jyun Ko

Institute of Applied Mechanics, National Taiwan University, 1, Sec. 4, Roosevelt Rd., Taipei 10617, Taiwan

* Corresponding author.

E-mail address: kcc@iam.ntu.edu.tw (K.C. Chen).

ABSTRACT

Fast-charging lithium-ion batteries (LIBs) may cause the formation of lithium metal deposits, known as lithium plating, on the anode, which not only reduces battery capacity but also increases the risk of internal short circuits, posing safety hazards. However, determining the onset of lithium plating solely from full-cell data of commercial LIBs, without disassembly, remains a challenge. To address this, we introduce a novel experimental method that generates a pseudo-P curve. This curve shares the same profile as the plating current curve (which can be simulated but not directly measured), varying only by a specific vertical scaling factor. It is found that the intersection of the two curves pinpoints the onset of lithium deposition. Constructing the pseudo-P curve involves determining the end time of lithium stripping and the corresponding net discharge capacity by varying the charging cutoff voltages. To validate the method's ability to correctly detect lithium plating onset, direct electrochemical simulations are conducted, showing a prediction error within 3.44% of total capacity. The correctness of this method is further supported by indirect experimental validation, based on the presence or absence of stripping signals when the charging duration is shorter or longer than the lithium plating onset point. Using the plating onset as a turning point, this method effectively guides charging strategies through current reduction at those turning moments. The proposed step-charging strategy

fully prevents lithium plating while achieving a Coulomb efficiency of 99.7% under the 2 C step-charging scenario.

Keywords: Lithium-ion batteries, Lithium plating, Onset of plating, Charging strategy.

1. Introduction

As modern technology rapidly evolves, the serious consequences of global warming and the growing societal focus on renewable energy have made electric vehicles (EVs) increasingly popular among consumers. Lithium-ion batteries (LIBs) are the primary energy storage technology for EVs, chosen for their impressive energy density, excellent voltage performance, long lifespan, and low self-discharge rates. However, LIBs encounter significant issues, particularly lithium plating, which tends to develop during fast charging [1], at low temperatures [2], when highly charged [3], and as the batteries age over time. These conditions can increase the local ion flux, slow lithium-ion diffusion, and reduce the availability of insertion sites in the anode, resulting in intercalation kinetics may become insufficient to accommodate incoming ion flux and thereby causing lithium deposit on the anode surface [4]. The accumulation of lithium metal on the anode can reduce capacity, raise the risk of internal short circuits, and compromise safety [5,6]. Therefore, detecting and preventing lithium plating has become a crucial area of research not only in battery technology but also in the development and safety of electric vehicles [7].

Several methods have been proposed to identify lithium plating, encompassing both invasive and non-invasive detection techniques [8,9]. Among the former methods, the reference electrode approach [10,11] allows for direct measurement of anode potential, facilitating accurate detection of lithium plating onset. However, due to its requirement for additional electrodes within the battery, this technique is predominantly limited to laboratory environments, rendering it unsuitable and potentially hazardous for deployment in commercial applications. Other invasive techniques, such as scanning electron microscopy (SEM) [12,13], provide detailed insights into battery structures but are costly and

demand extensive sample preparation, restricting their use to laboratory environments. Mass spectrometry titration (MST) [14], which analyzes components of the solid electrolyte interface (SEI), is another method; however, it is constrained by the need for high-precision calibration.

Various non-invasive techniques have also been developed. The most commonly used detecting methods include electrochemical impedance spectroscopy (EIS) [15-17], incremental capacity (IC) analysis [18,19], the relaxation voltage (RV) analysis [20,21], differential voltage (DV) analysis [22,23], differential pressure sensing (DPS) [24], and Coulombic efficiency (CE) monitoring [25]. Although EIS offers valuable insights by tracking the evolution of charge-transfer resistance, it typically requires extended relaxation times and costly equipment, which restricts its real-time applicability. Advancements such as dynamic EIS have mitigated these limitations by permitting continuous frequency-domain analysis during the charging phase [17,26]. IC, RV, and DV analysis can indirectly estimate lithium plating based on the voltage-time curves; however, the accuracy for pinpointing the onset of plating has not yet been fully confirmed. DPS is able to detect the subtle internal pressure changes associated with electroplating, but is highly susceptible to external interference and demands precise calibration. CE analysis is another non-invasive method that detects lithium plating by tracking inefficiencies during charge/discharge cycles. While simple and accessible, its sensitivity is limited, particularly in distinguishing plating from other aging effects.

To analyze and forecast lithium plating, modeling and data-driven approaches are becoming the booming trend [27]. Physically-based electrochemical models (e.g., a pseudo-two-dimensional (P2D) model [28], a multi-scale particle-level deposition-stripping model [29,30], a mathematical overcharge model [31], and a volume expansion-based detection model [32]) provide a theoretical framework to simulate lithium deposition under various charging conditions. While these models can accurately estimate the plating overpotential and lithium distribution, they require extensive parameterization of the cell's internal state and considerable computational resources. On the other hand, machine learning (ML) models [33] use large datasets such as voltage, current, and temperature to predict electroplating

risks. While ML approaches hold promise for enabling point-of-care diagnostics, their predictive accuracy depends heavily on the quality and diversity of the training data and they often lack interpretability, limiting their acceptance in safety-critical battery management systems. Overall, these model-related methods are valuable tools for understanding and tackling lithium plating, though they are currently more applicable for research and development than for direct commercial application.

To address the limitations and challenges mentioned above, this study proposes a pseudo-P curve method that integrates full-cell direct measurement data with electrochemical simulations to determine the onset of lithium plating. The theoretical foundation of this method is thoroughly explained, and its validity is confirmed through simulations and full-cell experiments. This method also supports multi-stage constant current (MSCC) charging strategies, enabling higher charging rates while completely eliminating lithium plating, as validated by model-based [34], data-driven [35], and experimental studies [36,37]. Table 1 summarizes the strengths and limitations of commonly used lithium plating detection methods with respect to five key criteria: battery disassembly, predictive capability, onset identification, compatibility with charging strategies, and suitability for real-time battery management systems (BMS). While most conventional techniques fail to satisfy all criteria simultaneously, the proposed method meets every benchmark, highlighting its potential for practical deployment in embedded BMS platforms.

The main contributions of this study can be summarized as follows:

(1) Generation of the proposed pseudo-P curve using only full-cell signals: Full-cell experimental data are utilized to construct the pseudo-P curve, from which the onset of lithium plating is determined.

(2) Analysis of the relationship between the plating current curve (P curve) and the pseudo-P curve: Electrochemical simulations are performed to ensure the consistent ratio between the plating amount during charging and the net discharge capacity during discharging.

(3) Application of step-charging strategies: The onset of lithium plating is used as the transition point to switch the current magnitude, leading to the proposal and evaluation of step-charging protocols.

The structure of this paper is organized as follows. Section 2 introduces the methodology for constructing the pseudo-P curve and its ability to predict the onset of lithium plating. Section 3 outlines the details of the experiment and data processing. Section 4 presents the experimental results, validates the prediction of plating onset, and discusses step-charging strategies based on the onset of plating. Section 5 gives the conclusion of this study.

Table 1

Methods for detecting lithium plating with various pros and cons.

Method	Ref.	Feature	No need of disassembly	Predictive ability	Onset prediction	Charging strategy	Suitable for BMS
Reference electrode	[10]	Anode potential	✗	✗	✓	✓	✗
SEM	[12]	SEM images	✗	✗	✗	✗	✗
MST	[14]	Correlation analysis	✗	✗	✓	✗	✗
EIS	[15]	C_{dl}, R_{CT}, τ_{CT}	✓	✗	✓	✓	✗
IC	[18]	IC curve peaks	✓	✗	✓	✓	✓
RV	[20]	dV/dt and current plateau	✓	✗	✗	✗	✓
DV	[22]	dV/dQ valley	✓	✗	✗	✗	✓
DPS	[24]	dP/dQ fluctuation	✓	✗	✓	✓	✗
CE	[25]	Loss deviation	✓	✗	✗	✗	✓
P2D	[28]	η or C_{max}	✓	✓	✓	✓	✗
ML	[33]	V, T, I features	▲	✓	✓	✓	△
Pseudo-P curve	This work	dV/dQ valley, net discharge	✓	✓	✓	✓	✓

Notes: ✓ represents "yes; ✗ denotes "no"; ▲ means both "yes" and "no" depending on cases; △ relies on model complexity and system constraints.

2. Methodology

The flowchart for detecting lithium plating and optimizing charging strategies is shown in Fig. 1. The process begins with theoretical considerations—starting from overpotential-driven plating,

progressing to plating current, and ultimately aiming to estimate the plating amount through voltage signals observed during the charge/discharge cycle. Electrochemical simulations are then conducted to support the theoretical framework and validate the proposed pseudo-P curve. At the next stage, the experimental voltage signals are employed to construct the pseudo-P curves at three different charging C-rates, enabling estimation of the onset of lithium plating. After detecting plating, we use this information to develop step-charging protocols. By implementing stepwise reductions in C-rate at identified lithium plating onsets, the proposed strategy effectively minimizes lithium plating while maintaining high Coulombic efficiency.

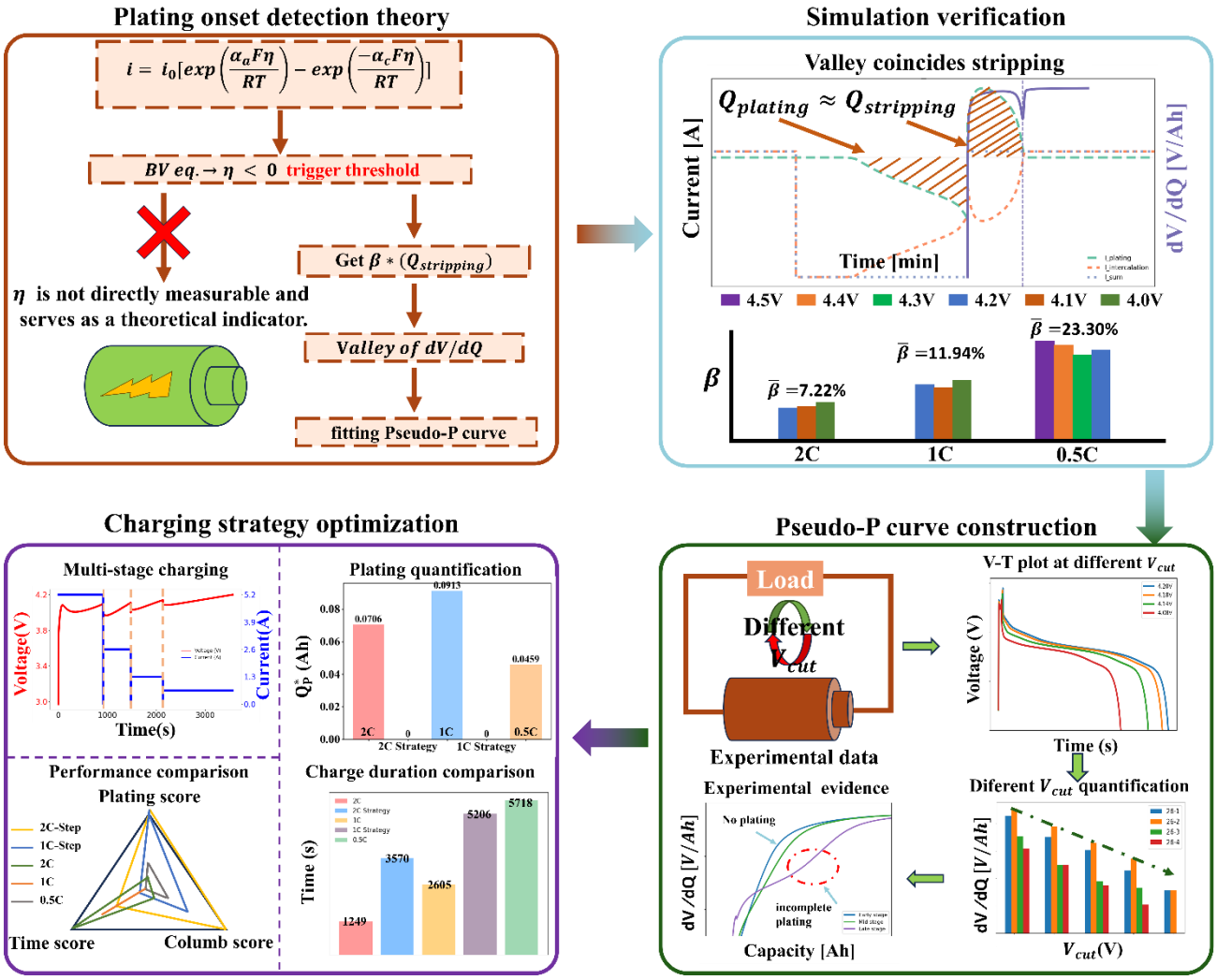

Fig. 1. Flowchart for detecting lithium plating and recommending charging strategy.

2.1. Theoretical thinking

When the plating overpotential—defined as the electrochemical potential difference between the anode surface and the electrolyte relative to the Li^+/Li redox potential—becomes negative (below 0 V versus Li/Li^+), conditions become thermodynamically favorable for lithium metal deposition [38,39]. Therefore, the overpotential serves as an indicator of the onset of lithium deposition. A key challenge is whether this potential can be monitored in commercial LIBs without disassembling the cell to insert a reference electrode. To investigate this, we begin with the classical Butler–Volmer (BV) kinetics, which governs the charge transfer rate of electrode reactions. Under charging conditions, the total local reaction current density at the anode is the sum of two components: the lithium-ion intercalation current density j_1, and the lithium metal plating current density j_2 [38-41]:

$$j = j_1 + j_2 \tag{1}$$

Both components can be expressed using the modified BV equations:

$$j_1 = j_{0,1}\left[exp\left(\frac{\alpha_{a,1}F\eta_1}{RT}\right) - exp\left(\frac{-\alpha_{c,1}F\eta_1}{RT}\right)\right] \tag{2}$$

where $j_{0,1}$ is the exchange current density for the intercalation reaction, $\alpha_{a,1}$ and $\alpha_{c,1}$ are the anodic and cathodic transfer coefficients (typically both 0.5), and η_1 is the overpotential for intercalation.

$$j_2 = j_{0,2}\left[exp\left(\frac{\alpha_{a,2}F\eta_2}{RT}\right) - exp\left(\frac{-\alpha_{c,2}F\eta_2}{RT}\right)\right], \quad \text{for charging } (\eta_2 < 0) \tag{3}$$

Here, $j_{0,2}(= Fk_{pl}c_e)$ is the exchange current density for the lithium plating reaction, F is Faraday constant, k_{pl} is the reaction rate constant of the plating reaction, c_e is the lithium ion concentration in the electrolyte solution, and $\alpha_{a,2}$ and $\alpha_{c,2}$ are typically unequal (e.g., 0.3 and 0.7, respectively), reflecting the asymmetry of the plating mechanism. In addition, it is noted that during the transition

from charging to discharging, the plating current density j_2 is interpreted as the stripping current density:

$$j_2 = j_{0,3}\left[exp\left(\frac{\alpha_{a,2}F\eta_2}{RT}\right) - exp\left(\frac{-\alpha_{c,2}F\eta_2}{RT}\right)\right], \quad \text{for discharging } (\eta_2 > 0) \tag{4}$$

where $j_{0,3}(= Fk_{pl}c_{Li})$ is the exchange current density for the lithium stripping reaction and c_{Li} is the lithium ion concentration on the anode surface [42].

The BV equations can be simplified and tailored to specific charging scenarios or targeted charging ranges. When the plating overpotential drops below zero during the charging process ($\eta_2 < 0$), lithium plating begins, coinciding with the initiation of plating current [40,41]. Accordingly, identifying the zero plating overpotential point is equivalent to pinpointing the exact moment when plating current first starts to flow, effectively shifting the above challenge to monitoring the plating current. The following two-step idea is now proposed to extract plating current data from experiments conducted on commercial LIBs.

STEP I: Since reversible lithium plating can be completely stripped during discharge, it appears possible to determine the total amount of plated lithium by analyzing the discharge voltage profile of a full cell. Voltage differential (dV/dQ) analysis, derived from processing the voltage signal, is recognized as a highly sensitive, non-destructive technique commonly employed in LIB research, especially for detecting lithium deposition and stripping processes [43]. The valleys in the dV/dQ curve reveal the changes in voltage rate as lithium ions enter or exit the electrode surface [44,45]. Consequently, these distinctive valley points offer crucial information for the onset and completion of lithium plating and stripping, helping to identify the timing of these processes. Through examination of these valleys, it may be expected that the amount of reversible lithium plating occurring over a specific time interval can be estimated.

STEP II: Given the total amount of lithium plating, we can calculate the average plating current

between any two timepoints, which serves as an indicator for determining when lithium plating begins to occur. However, the feasibility of our proposed idea—quantifying reversible lithium plating amounts and estimating average plating currents using discharge measurement data—requires careful validation, which will be comprehensively examined in the following section.

2.2. Electrochemical simulation of plating current

To investigate the possible relationship between the charge/discharge curves and the amount of lithium plating, we conduct electrochemical simulations utilizing the open-source Python Battery Mathematical Modeling (PyBaMM) package available on GitHub [46]. Thanks to its flexibility and computational efficiency, this package has recently gained widespread use in battery modeling [47,48]. The parameter dataset for the LG INR M50T ($LiNiMnCoO_2$, NMC) cell is utilized in the modeling [49], along with parameters related to lithium plating kinetics [50,51].

The simulations consider lithium plating as a competing side reaction that follows a thermodynamic criterion. Specifically, plating only begins when the local overpotential against the Li^+/Li redox potential drops below zero ($\eta_2 < 0$), as shown in Eq. (3). The corresponding plating and stripping currents are calculated using overpotential-dependent BV expressions, allowing a continuous transition between deposition and dissolution without the need to manually switch reaction modes. Aging-related effects such as SEI layer growth, pore clogging, or lithium trapping are not taken into account in the present simulations, which may cause slight deviations in the actual onset of lithium plating in real LIBs. Assuming fully reversible lithium plating, the simulations are carried out under consistent conditions at 0 °C, beginning with a 0.05 C constant-current (CC) discharge to 2.5 V, followed by 1 C charging to three different cut-off voltages (4.00 V, 4.10 V, and 4.20 V), and ending with a second 0.05 C discharge to 2.5 V.

Our simulations clearly demonstrate the mechanism underlying the transition of lithium ions from intercalation to plating, followed by re-intercalation. As illustrated in Fig. 2, the 1 C charging and 0.05

C discharging processes can be divided into three stages. In the early stage of charging, lithium ions intercalate into the graphite anode. As charging proceeds and the intercalation capacity gradually saturates near the anode surface, lithium plating occurs during the later phase of charging. When discharge at a low C rate begins, lithium ions from the plated lithium are first stripped into the electrolyte, then driven by concentration gradients and electric potential differences to migrate back into the anode.

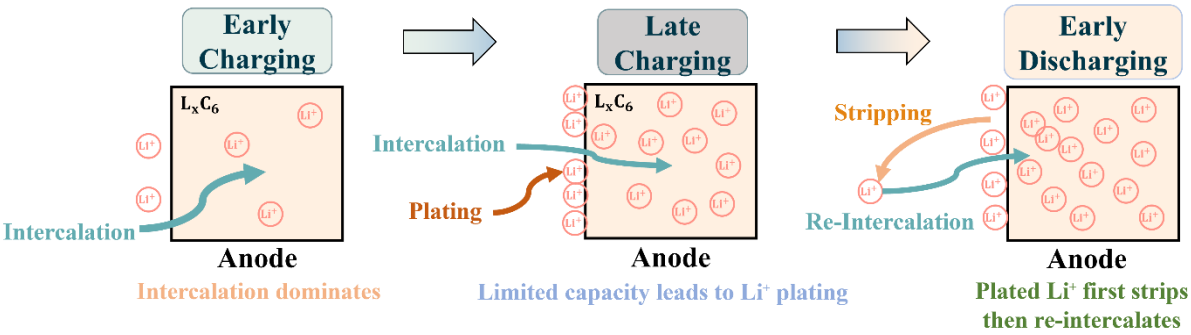

Fig. 2. Schematic of lithium-ion movement during early and late charging, as well as early discharging.

Fig. 3(a) displays the voltage evolution of a representative simulation cycle. The four key time points, T_0, T_A, T_B, and T_C, are specially highlighted, corresponding to the first transition between charge and discharge, the onset of lithium plating, the second transition between charge and discharge, and the end of lithium stripping, respectively. Fig. 3(b) presents the time evolutions of the currents associated with lithium plating (blue line), intercalation (orange line), and their combined total (green line). Note that, in the simulations, the current density in anode is transformed into current by multiplying the active area, which is evaluated by $(3\varepsilon_s/R_p)LA$ with ε_s, R_p, L, and A being the volume fraction of solid particles, particle radius, electrode thickness, and cross sectional area, respectively [52].

Symbols (i) through (vi) signify the six current curves during the time intervals between T_A and T_B, and between T_B and T_C. To be explicit, Symbol (i) denotes the plating current curve (referred to as the P curve hereafter), which emerges during the late stage of charging. Symbol (ii) refers to the

stripping current curve observed at the beginning of discharge, when lithium metal starts to dissolve back into the electrolyte. Symbol (iii) indicates the curve for the intercalation current during charging. This current initially equals the total current but gradually declines as plating commences, highlighting the trade-off between intercalation and plating needed to maintain a constant total current. Symbol (iv) represents the re-intercalation current curve in discharging phase, where stripped lithium ions migrate back into the graphite. Symbol (v) stands for the curve for the total current, which stays constant (1 C) throughout the process by the definition of CC charging. Symbol (vi) is the curve for the net discharge current across the time period between T_B and T_C, which is the sum of the stripping (ii) and re-intercalation (iv) currents, and it remains nearly constant (0.05 C) to maintain the balance of the total current.

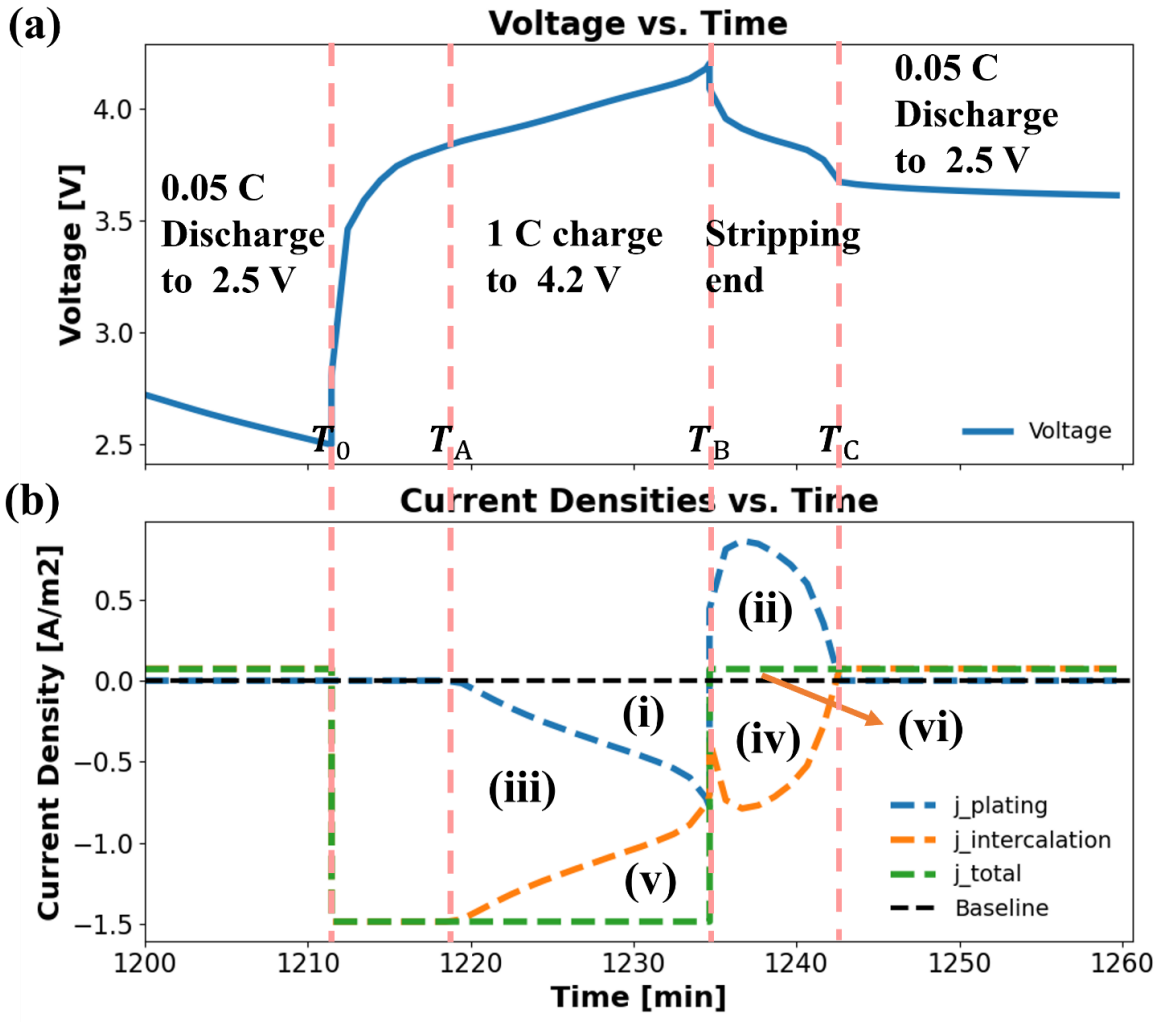

Fig. 3. (a) Voltage profile of a 0.05 C–1 C–0.05 C cycle. (b) Time dependent currents depicting lithium plating, intercalation, and the over sum.

Concerning the area analysis in Fig. 3(b), the area enclosed by the P curve between points T_A and T_B is equal in magnitude to the area under the blue line between T_B and T_C. This indicates that the total amount of lithium plating during charging is fully dissolved during discharging, assuming only reversible plating is considered. Moreover, during the discharge period from T_B and T_C, the difference between the absolute values of the areas enclosed by the blue and orange lines equals the area enclosed by the green line. This green-line area represents the net discharge capacity over the time interval from T_B to T_C, which can be directly obtained from experimental measurements.

The simulations also reveal that the end point T_C, at which the stripping current vanishes, nearly aligns with the valley point of the differential voltage dV/dQ curve during the discharging phase. This assertion, validating the use of the dV/dQ valley as a reliable marker for the end of lithium stripping, is shown in Fig. 4(a), which presents three scenarios with charging cutoff voltages of 4.0 V, 4.1 V and 4.2 V. As the time points T_B and T_C can be experimentally determined, the net discharge capacity can be measured under different charging cutoff voltages. Fig. 4(a) also illustrates that the plating current curves in the three scenarios follows the same trajectory. Specifically, at the same charging C rate but with different cut-off voltages of 4.0 V, 4.1 V, and 4.2 V, the P curve begins at the same time point (T_A) and follows the same path to reach different time points: $T_{B(4.0)}$, $T_{B(4.1)}$, and $T_{B(4.2)}$. This property is essential for the subsequent analysis, as it allows the determination of the starting time point T_A by examining the unique P curve.

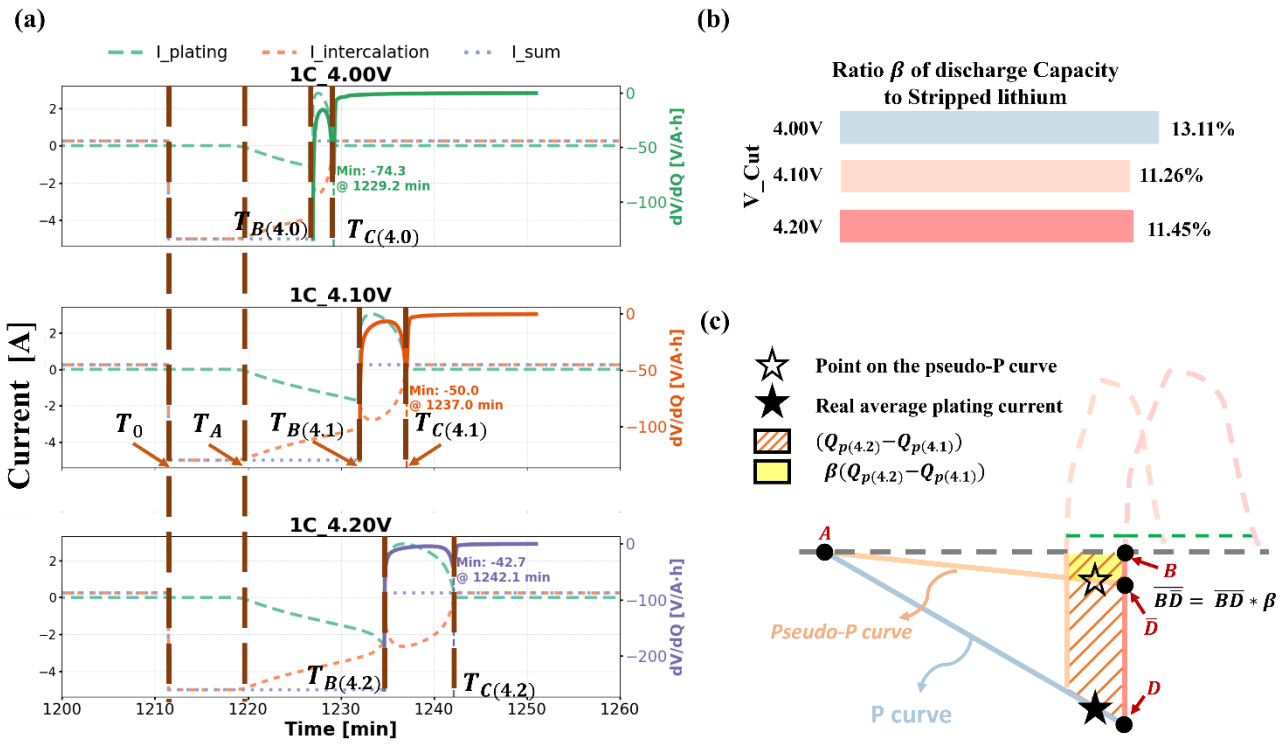

Fig. 4. (a) dV/dQ valley marks the end of lithium stripping. (b) Ratio β of discharge capacity to stripping lithium amount at three different charging cutoff voltages. (c) The P curve and its β-ratio-modified pseudo-P curve, intersecting at time T_A (point A).

The P curve could potentially be constructed once at least a few points on it are identified. To clearly interpret the geometric significance of the P curve, we define three points A, B, and D in Fig. 4(c) as the point on the P curve at T_A, the point on the baseline at T_B, and the point on the P curve at T_B. The area enclosed by the points A, B, and D, which corresponds to the absolute value of the area between the P curve and the baseline within the interval between T_A and T_B, represents the amount of lithium plating Q_P (also the same as the lithium stripping between T_B and T_C). However, this area Q_P cannot be directly obtained from measurements, making it impossible to generate the points on the P curve and thus creating an obstacle to producing the P curve. To avoid this obstacle, a novel approach for determining the plating onset T_A is introduced here, using a proposed pseudo-P curve.

First, we evaluate the ratio (called β ratio) of net discharge capacity to the amount of stripped lithium during the discharge process between T_B and T_C. Here, the net discharge capacity—an

experimentally measurable quantity—is represented by the area (=$I_{total}(T_C - T_B)$) under the green line in Fig. 3(b), whereas the amount of stripped lithium, which cannot be directly measured experimentally, corresponds to the area between the blue line and the baseline. As shown in Fig. 4(b), the β ratio consistently stays around 12% in the simulations, nearly independent of the charging cutoff voltage. Owing to the consistent β ratio, the amount of stripping (or plated) lithium Q_P can be inferred from the measurable net discharge capacity Q_P^*, where Q_P^* is defined as βQ_P.

Second, let us take the cutoff voltage of 4.2 V as an example and focus on the P curve between T_A and T_B. Instead of directly evaluating the lithium plating amount Q_P, we seek a region within T_A and T_B that has an area equal to Q_P^* $(= \beta Q_P = I_{total}(T_C - T_B))$. This can be achieved by generating a new curve, called the pseudo-P curve, which resembles the P curve but is modified by the β ratio in the vertical direction. As shown in Fig. 4(c), the absolute value of the area between the pseudo-P curve and the baseline over the interval from T_A and T_B—enclosed by points A, B, and $\bar{D}$—represents the measurable discharge capacity $Q_{P(4.2)}^*$, where $\bar{D}$ is the point on the pseudo-P curve at time T_B. In addition, the pseudo-P curve also passes through the same point A, which is exactly the target we aim to determine.

Third, to implement the generation of pseudo-P curve from the simulation perspective, several points on this curve must be determined, allowing its construction based on the measurable net discharge capacity. This can be readily achieved by using two cutoff voltages—such as 4.2 V and 4.1 V—as an illustrative example. It should be noted from Fig. 4(c) that the slashed area is $(Q_{P(4.2)} - Q_{P(4.1)})$, with its yellow portion corresponding to $(Q_{P(4.2)}^* - Q_{P(4.1)}^*)$. Thus, the points on the P curve and the pseudo-P curve at time $(T_{B(4.2)} + T_{B(4.1)})/2$, symbolled by "★" and "☆", can be approximately located by evaluating $(Q_{P(4.2)} - Q_{P(4.1)})/(T_{B(4.2)} - T_{B(4.1)})$ and $(Q_{P(4.2)}^* - Q_{P(4.1)}^*)/(T_{B(4.2)} - T_{B(4.1)})$, where $Q_{P(4.2)}$ and $Q_{P(4.1)}$ denotes the total amounts of lithium plating when the charging ends at 4.2 V and 4.1 V, respectively. Similarly, other points on the

two curves can be determined using the same procedure.

In conclusion, the proposed pseudo-P curve offers two main advantages. (i) It closely resembles the P curve and shares a common intersection point at time T_A, which marks the onset of lithium plating, (ii) It can be determined using detectable full-cell data. Therefore, even without knowing the exact lithium plating amount and the β ratio, the onset time of lithium plating T_A can still be inferred by extrapolating points on the curve—each derived from the measurement of T_B, T_C, and net discharge capacity $I_{total}(T_C - T_B)$ within the interval between T_B and T_C.

3. Experiment and data processing

Previous electrochemical studies indicated that lithium plating initiates during CC charging when the anode overpotential drops below 0 V(vs. Li/Li$^+$). As CC charging continues, the plating current increases accordingly. The goal of this experiment is to determine the moment when the plating current starts using only full-cell measurement data, where the differences in the discharge capacity between any two selected data points are evaluated to derive the pseudo-P curve.

3.1. Experimental setup

Four brand-new commercial Samsung 18650-26J cylindrical NMC lithium-ion batteries, labeled 26-1, 26-2, 26-3, and 26-4, were tested using a Bio-Logic BCS-815 ultra-precision battery cycler and a Bio-Logic BH-1i commercial battery holder. All tests were conducted in a controlled temperature environment using an ABT-CH-R60 thermal chamber. The experimental procedures include activation, aging, state of health (SOH) evaluation, and lithium plating tests, as illustrated in Fig. 5(a).

3.2. Various tests

Activation—Before the experiment, batteries underwent an activation process to stabilize the solid electrolyte interphase (SEI). Each cell was charged using a CC protocol at 0.5 C up to 4.2 V,

followed by a constant voltage (CV) phase until the current decreased below 0.05 C, and then discharged at a CC of 0.2 C down to 2.75 V. Additional five 1 C charge-discharge cycles were carried out to accelerate SEI stabilization and establish a consistent base capacity matching the nominal value.

SOH measurement—To consider the possible minor capacity loss from repeated cycling of a single battery at low temperatures, the SOH was evaluated following the activation process and after each plating test. Each SOH test involved a 0.5 C CC charge to 4.2 V, a CV charge with a cutoff current of 0.05 C, a 1-hour rest, and a 0.2 C discharge to 2.75 V. The resulting discharge capacity was normalized by the nominal capacity (2600 mAh) to define the SOH. To eliminate the SOH-induced bias in charging time (CT), a correction factor was applied to ensure consistency across tests

$$SOH_{avg} = \frac{(SOH_1 + \cdots + SOH_n)}{n} \tag{5}$$

$$CT_{i,corr} = \frac{CT_i}{SOH_i} \times SOH_{avg} \tag{6}$$

where each test refers to a single charge–discharge cycle, SOH_i is the SOH value of test i, SOH_{avg} is the average SOH across all test cases, CT_i represents the observed CC charging time, and $CT_{i,corr}$ means the normalized charging time for use in plating current estimation. n denotes the number of distinct charge/discharge test cases conducted on the same battery under varying cut-off voltages, which is 4 for 2 C charging and 5 for 1 C charging.

Lithium plating test—Two plating test protocols were conducted at 0 °C. All cells were initially discharged to 2.75 V at 0.05 C to standardize initial conditions, with voltage, current, capacity, and time recorded every five seconds during subsequent charging and discharging. The procedure of this test is outlined in Fig. 5(b).

(1) Pseudo-P curve construction test: After the initial discharge, the cells were charged at 0.5 C, 1 C, or 2 C to different cutoff voltages (4.08–4.20V) and then discharged at 0.05 C to 2.75 V. The onset of lithium deposition was determined by performing the dV/dQ analysis on the second discharge. These results were used to establish the pseudo-P curves under different charging conditions.

(2) Strategy verification test with 50% initial SOC: After the initial discharge, the cells were pre-

charged to 50% SOC at 0.2 C, rested for 1 h, then charged at 0.5–2 C to 4.2 V and discharged again at 0.05 C. Based on prior findings that plating initiates above 50% SOC at high C-rates, this specific SOC was chosen to access the multi-stage constant current (MSCC) strategy, which reduces current after 50% SOC to mitigate plating.

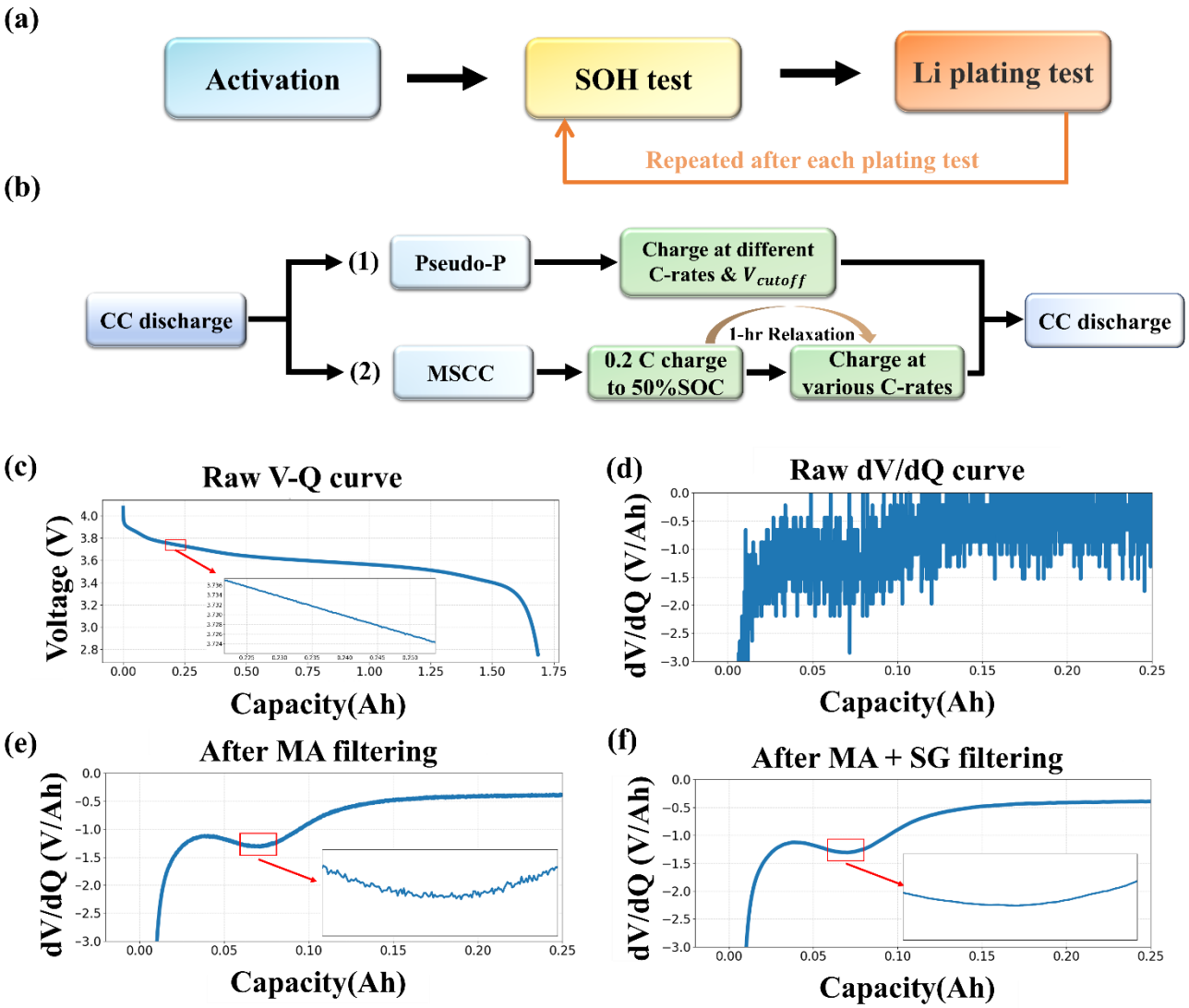

Fig. 5. (a) Schematic of the three experimental works. (b) Detailed workflow of the activation, SOH evaluation, and plating tests. (c) Raw V–Q curve with small fluctuations. (d) dV/dQ curve from the raw data. (e) After MA filtering (window: 80). (f) After MA and Savitzky–Golay filtering (order 3, window: 31).

3.3. Signal smoothing

The accurate identification of the valley point in the dV/dQ curve during discharge is critical, as this point signifies the end of lithium stripping and enables precise determination of the net discharge capacity βQ. Following established procedures that highlight the importance of signal preprocessing with smoothing filters [53], we implement a two-step smoothing process as shown in Fig. 5(c)–(f). This process effectively reduces noise amplification when performing numerical differentiation of voltage–capacity (V–Q) experimental data.

Fig. 5(c) shows the raw V–Q curve in discharge with subtle fluctuations, where minor fluctuations lead to a noisy dV/dQ profile in Fig. 5(d), making it difficult to distinguish critical features such as the lithium stripping valley. Initially, background noise was reduced using a moving average (MA) filter with an 80-point window as depicted in Fig. 5(e) [54]. Subsequently, a third-order Savitzky-Golay (SG) filter with a 31-point window was applied to eliminate remaining fluctuations [55]. Fig. 5(f) displays the final outcome, showing a smooth and stable dV/dQ curve with well-preserved valley features, enabling reliable identification.

4. Results and discussions

4.1. Points on the pseudo-P curve

As shown in Fig. 3 and 4, each discharge–charge–discharge process conducted at a designated charging cutoff voltage yields a distinct set of parameters: a specific CC charging time (T_B) signifying the transition from charging to discharging, a corresponding reversible lithium capacity (Q_P), a specific moment (T_C) marking the end of lithium stripping, and a quantifiable net discharge capacity (Q_P^*). Both T_C and Q_P^* can be extracted from the dV/dQ curve, which is the first derivative of the voltage-charge curve during the second discharge process. By changing the charging cutoff voltage, the relationship between the Q_P^* and the charging time T_B can be established. Fig 6(a) displays this relationship when the charging C-rate is 1 C as well as the voltage evolution. It should be emphasized that each Q_P^* value at a given time T_B—corresponding to a specific charging cutoff voltage—is derived from the

subsequent discharge phase and represents the net discharge capacity within the T_B-T_C interval.

With these Q_P^* and their associated T_B, one can evaluate $\Delta Q_P^*/\Delta T_B$ for two different T_B values to construct the pseudo-P curve. According to our simulations shown in Fig. 3(b) and 4(a) and the literature [56], the plating current exhibits approximately linear behavior under small overpotential conditions. Therefore, it is reasonable to fit these data points as a straight line that intersects the baseline at the onset of lithium plating, T_A. To verify repeatability under the same test conditions, four batteries (Cells 26-1 to 26-4) are tested at 0 °C, with Cells 26-1 and 26-2 charged at 2 C, and Cells 26-3 and 26-4 at 1 C. As shown in Fig. 6(b)-6(e), while there are some differences in predicting T_A when the current extrapolates to zero for individual batteries, the capacity deviation between the two batteries is only 1.00% under 2 C charging (Cell 26-1 and 26-2) and 3.33% under 1 C charging (Cell 26-3 and 26-4).

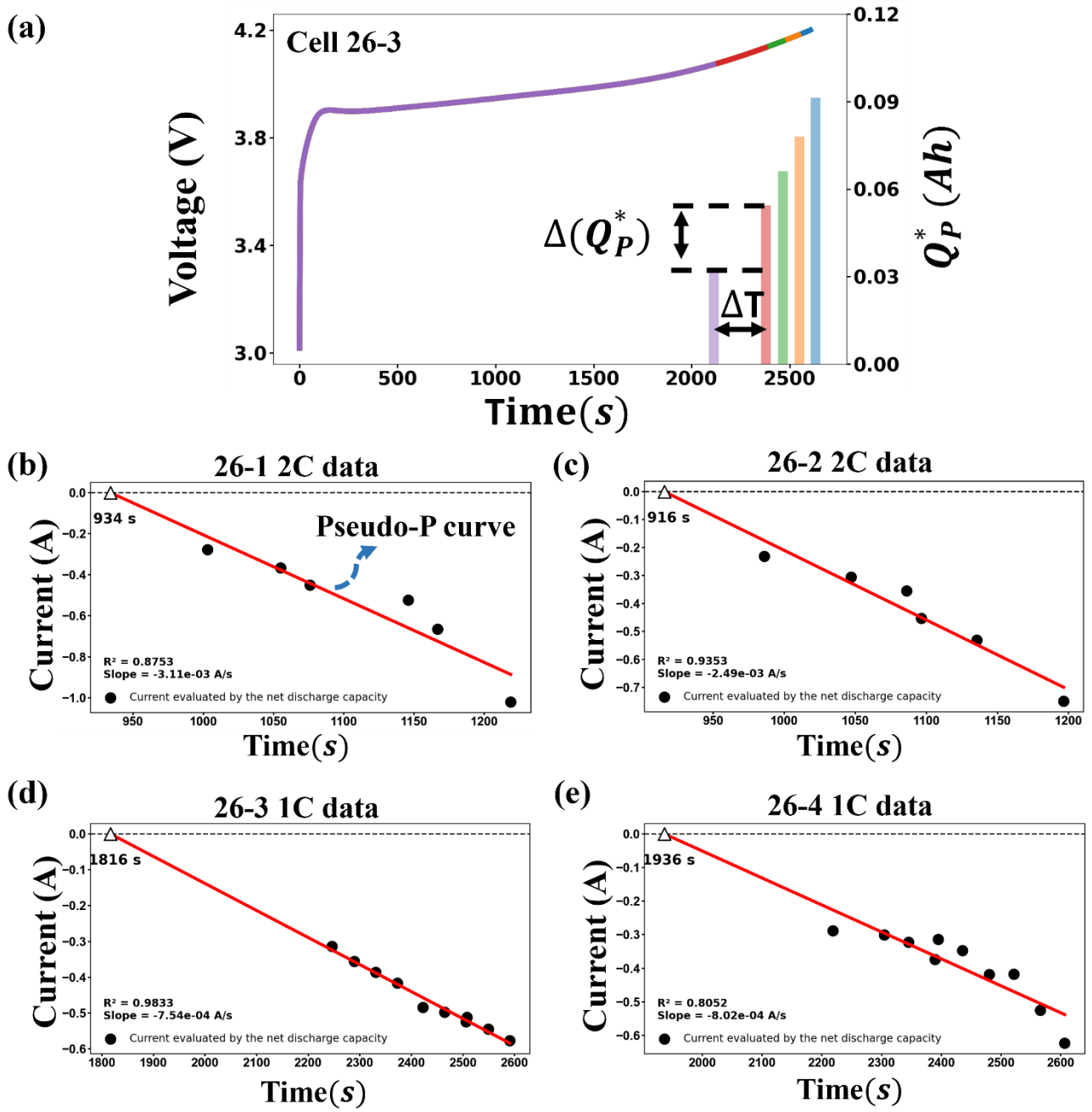

Fig. 6. (a) Voltage and Q_P^* versus T_B when the charging C-rate is 1 C. Pseudo-P curve construction at 0 °C for different cells: (b) Cell 26-1, (c) Cell 26-2, (d) Cell 26-3, and (e) Cell 26-4.

4.2. Check of T_A using neighboring points

The time point T_A identified from the proposed linear pseudo-P curve is now verified to correctly indicate the onset of lithium plating, without battery disassembly. Additional experiments are

conducted at 0 °C using identical charging/discharging protocols but with charging durations that deviate from the T_A value.

As illustrated in Fig. 7, selecting a 1 C charging rate and a charging duration of 1827 s results in a dV/dQ curve during the discharging phase that exhibits no signs of lithium plating, consistent with the pseudo-P curve's prediction. When the charging duration is less than 1827 s, no any indicators of lithium plating are observed, further confirming the absence of lithium deposition. However, once the charging time surpasses 1827 s, the dV/dQ curve begins to shift or deflect, signaling the occurrence of lithium plating during the preceding charging phase. This deviation becomes increasingly pronounced as the charging time continues to increase. A similar pattern is observed under 2 C charging conditions, with lithium plating initiating at 916 s (see Fig. 6(c)). Beyond this point shown in Fig. 7(b), the signs of plating become progressively more pronounced.

Fig. 7(a) demonstrates that despite T_A (=1816 s) being identified as the lithium plating onset for Cell 26-3 (see Fig. 6(d)), the dV/dQ curve in the discharging phase following this 1816-s charging duration exhibits minimal indication of plating. Even with a charging time of 1947 s (early plating stage), the dV/dQ curve displays only partial or incomplete plating characteristics [57]. This observation, also evident in Cell 26-2 with 2 C charging (see Fig. 7(b)), explains why the points used to generate the pseudo-P curve need be positioned away from the onset point occurring at time T_A to ensure they can be clearly identified in experiment.

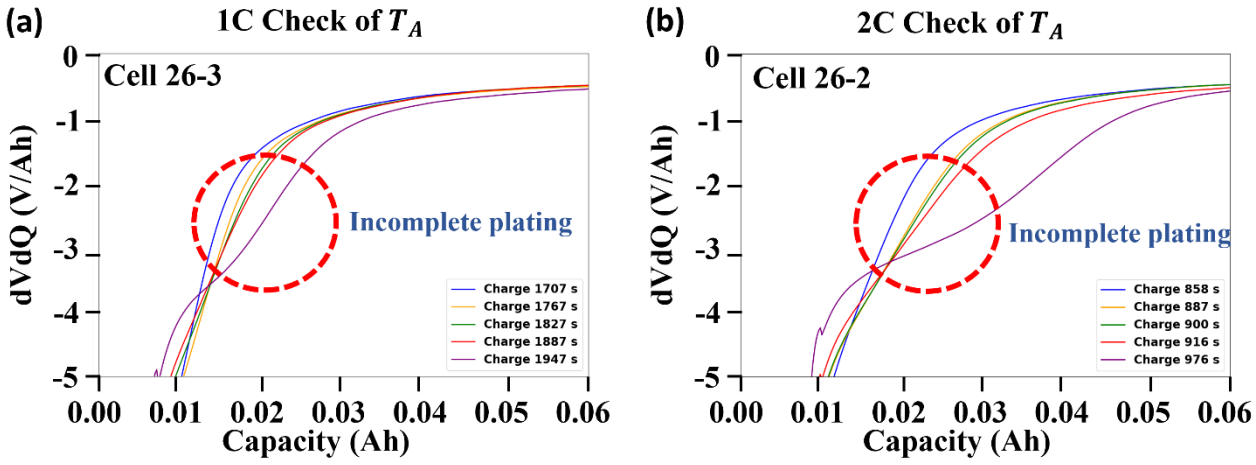

Fig. 7. dV/dQ curves in the discharging phase following charging at 0 °C with (a) 1 C-rate and (b) 2 C-rate, shown for various charging durations. Note that the experimental onset times T_A for (a) and (b) are 1816 s and 916 s, respectively.

4.3. Simulation validation

To further validate the onset of lithium plating predicted by the proposed pseudo-P curve approach accompanied with experimental full-cell data, the simulation model in PyBaMM, which is based on the P2D theory, is employed again. Although the electrochemical parameters in the simulation do not precisely match those of the tested cell, the simulation successfully reproduces key battery responses. Specifically, the PyBaMM model provides valuable insights into mechanisms involved in challenging scenarios such as low temperatures, high currents, overcharging, and material deterioration—conditions that are dangerous and difficult to quickly reproduce in experimental settings.

These simulations estimate the lithium plating, stripping, and net charging/discharging currents by analyzing deposited/stripped lithium capacity and specific time points (T_B, T_C), using the methodology described in Section 4.1. All simulations are performed at 0 °C with 1 C CC charging to various cut-off voltages (4.00 V, 4.05 V, 4.10 V, 4.15 V, 4.20 V) to align with our experimental conditions.

Fig. 8(a) displays the time evolutions of plating amount under various charging cutoff voltages, with the "▼" symbol pinpointing the end of stripping (T_C) for the three selected scenarios. These time moments also correspond to the valleys points on the respective dV/dt curves during discharging, as shown in Fig. 8(b). Since the simulations define the initial charging time as zero, the total charging duration for each case with different cutoff voltages corresponds to the value of T_B, as listed in Table 2, which also includes the maximum plating capacities. Fig. 8(c) gives the averaged plating currents across the anode thickness during the charging/discharging process, where the onset of lithium plating T_A occurs at 459 s in this simulation. Based on the simulation data for T_B, and T_C, and the net discharge

capacity during discharging, the coordinates of the points marked as "☆" in Fig. 4(c) can be determined. Linear fitting of this set of points produces the pseudo-P curve displayed in Fig. 8(d), yielding the simulated T_A values of 584 s, respectively. Although there appears to be a discrepancy between T_A (459 s) from the plating current and that derived from the pseudo-P curve (584 s), the difference in total capacity is merely 3.44%. This also confirms the reliability of the proposed pseudo-P curve method for estimating the onset of lithium plating.

Table 2
PyBaMM simulation data.

Cut-off voltage (V)	Charge time (s)	Plating capacity (Ah)
4.2	1393.2	0.29337
4.15	1351.8	0.26628
4.10	1235.4	0.20412
4.05	1078.2	0.13444
4.00	933.6	0.08223

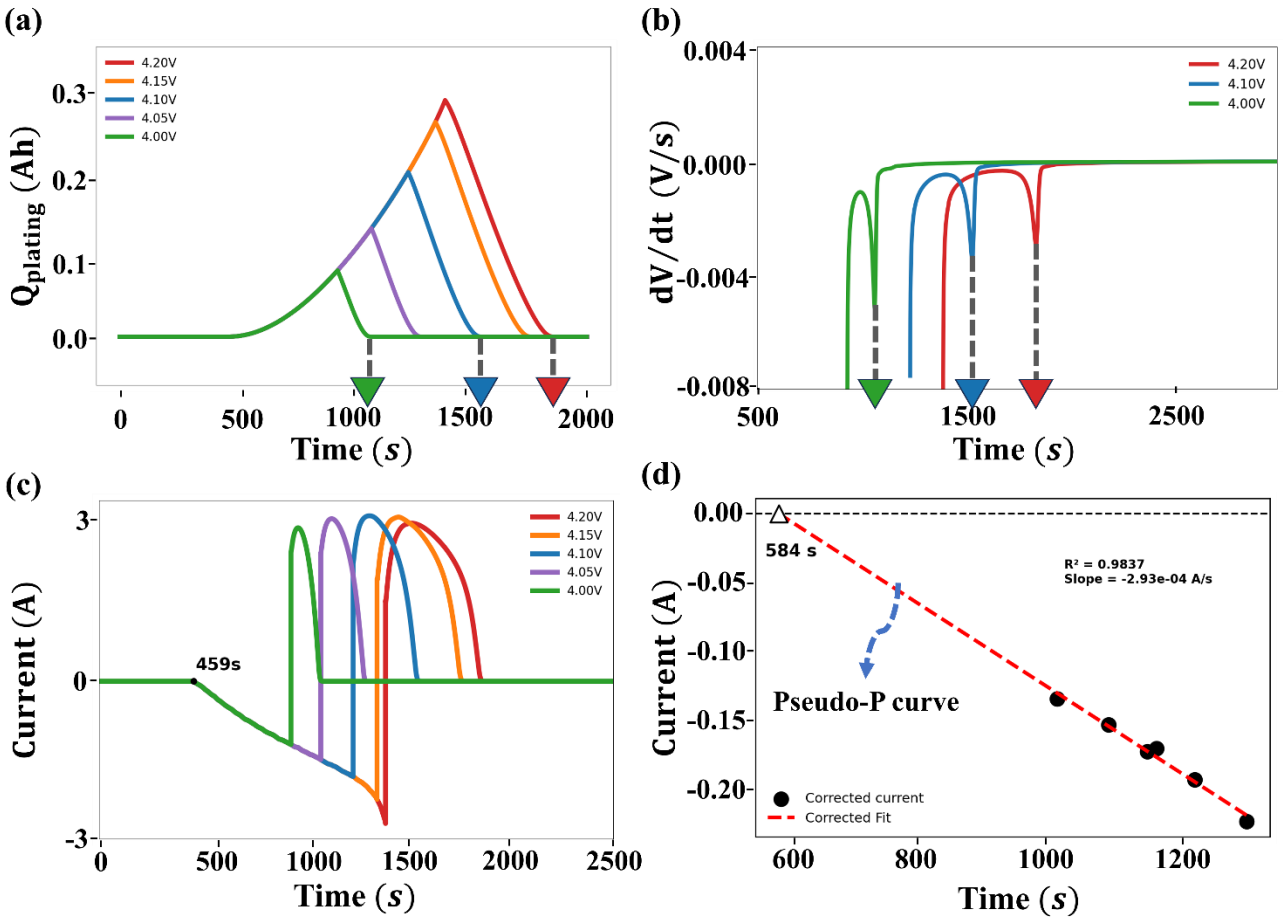

Fig. 8. (a) Simulated lithium plating deposition under 1C CC charging at 0 °C using the PyBaMM model under different charging cutoff voltages, (b) dV/dt curves during the charge/discharge process, (c) lithium plating currents, and (d) pseudo-P curve, entirely derived from the simulated data points.

4.4. Charging with lower C-rate

From the previous experimental analysis of the two charging rates (1 C and 2 C), it is anticipated that reducing the charging rate can delay the onset of lithium plating. To examine the impact of charging rate on the onset and duration of lithium plating, additional charging data are collected to examine the scenario where the charging C-rate is reduced to 0.5 C. As depicted in Fig. 9(a), the pseudo-P curve reveals that lithium plating at 0 °C begins at 5437 s, which roughly corresponds to 75.5% SOC, a value higher than the plating-onset SOC observed at higher charging C-rates. This can

be attributed to the reduction in polarization at lower charging C-rates, enabling the battery to reach a higher SOC before the lithium plating is triggered [58].

Once we identify both the onset time of lithium plating (T_A) from the pseudo-P curves and the moments when charging reaches the 4.2 V cutoff voltage (T_B), we plot the lithium plating duration (the interval from T_A to T_B) for all three charging rates (0.5 C, 1 C, and 2 C). Fig. 9(b) displays these experimental plating durations in terms of both charging time and SOC. It can be observed that as the C-rate of charging decreases, lithium plating begins later and at higher SOC.

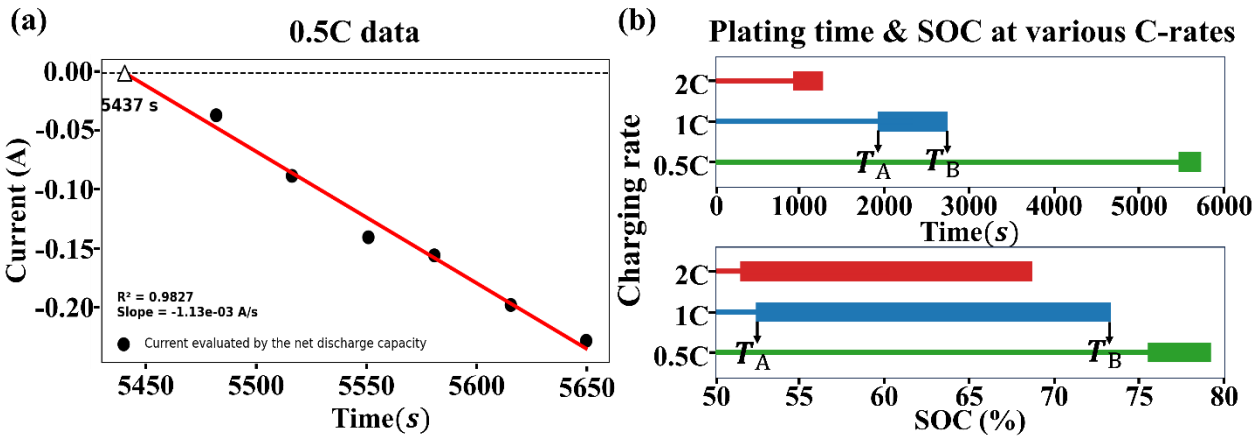

Fig. 9. (a) The pseudo-P curve generated by the experimental data points at 0 °C using 0.5 C charging current. (b) Plating durations in terms of charging time and SOC at 0 °C under three different C-rates.

4.5. Charging starting from 50% SOC

Fast-charging protocols commonly adopt high currents until reaching a specific SOC threshold, then reduce current to limit lithium deposition. To investigate this transition, we first charge the battery to an SOC of 50% at 0.2 C, and then continue charging at varying C-rates until the cutoff voltage is reached. The SOC = 50% is selected based on Fig. 9(b), where lithium plating occurs when the SOC exceeds 50% for the 1 C and 2 C charging cases. This analysis enables us to assess the effects of reduced charging currents after reaching specific SOC levels and determine the safe charging duration or capacity before reaching the next plating onset point.

The pseudo-P curves for the 1 C and 0.5 C charging following an initial SOC (SOC_0) of 50% at 0

°C are presented in Fig. 10, with the key observations outlined below. (i) At 1 C charging rate, lithium plating initiates at 560 s, corresponding to about 15.56% of the total capacity delivered to the battery by that time. (ii) Under 0.5 C charging, the plating onset is delayed to 1620 s, which permits approximately 22.51% of charge capacity. These observations suggest that, at the same initial SOC, a lower C-rate enables more charge to be delivered before lithium plating begins.

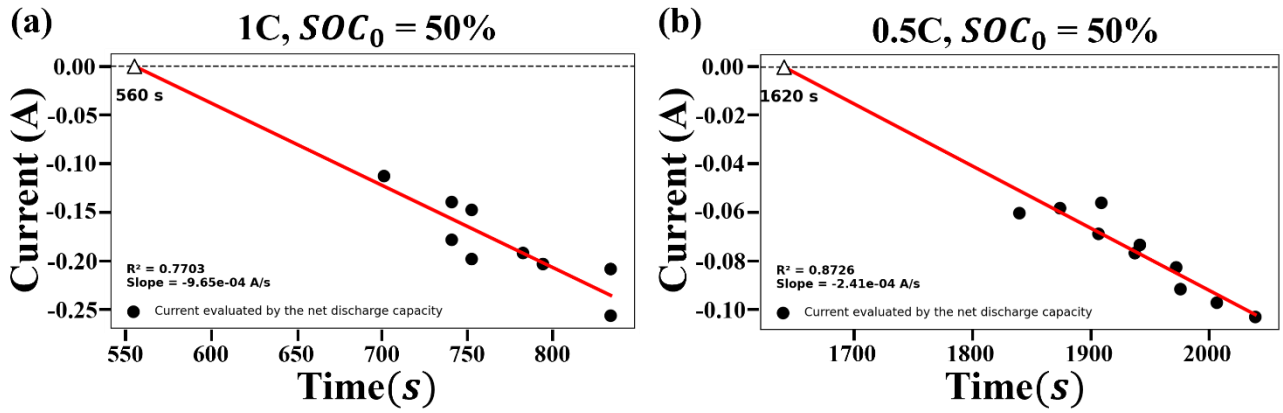

Fig. 10. Pseudo-P curves generated from data obtained when batteries with initial SOC of 50% at 0 °C are charged at (a) 1 C and (b) 0.5 C rates.

4.6. Charging strategy application

The proposed method allows us to detect the onset of lithium plating, enabling continued charging without plating by reducing current magnitude. To assess the performance of various charging protocols which involve the stepwise current reduction charging, we examine two variants of this charging approach: the 1 C step-charging strategy and the 2 C step-charging strategy.

Experimental data reveals that lithium deposition begins at 1816 s (SOC ≈ 50.44%) when charging the battery at 1 C from 2.75 V. Reducing the charging current to 0.5 C at this point postpones plating onset. Previous analysis indicates that charging at 0.5 C from SOC = 50% requires an additional 1620 s (reaching SOC ≈72.95%) before plating starts. The current is subsequently reduced to 0.25 C, enabling continued charging until reaching 4.2 V. A brief 5-s rest interval is introduced between current transitions to ensure smooth charging stage transitions. The procedure described above defines the 1 C

step-charging strategy (1 C→0.5 C→0.25 C). The 2 C step-charging strategy (2 C→1 C→0.5 C→0.25 C) follows a similar pattern, beginning with 2 C charging for 916 s (SOC ≈ 50.89%) before switching to 1 C for an additional 560 s (reaching SOC ≈ 66.44%). The current is then lowered to 0.5 C, continuing the charging process for 650 s (reaching SOC ≈ 75.47%), followed by a final decrease to 0.25 C until reaching 4.2 V. This stepwise reduction in current aims to control plating by maintaining positive overpotential throughout the entire charging process [59].

For a comparative analysis between conventional CC charging and stepwise current reduction charging, Table 3 summarizes several performance metrics—including total charging time, Coulombic efficiency, total charge capacity, total discharge capacity, and net discharge capacity between T_B to T_C—across various charging protocols: traditional 2 C, 1 C, and 0.5 C methods, as well as 1 C and 2 C step-charging strategies. Note that the net discharge capacity between T_B to T_C serves as a measurable indicator for determining whether lithium plating occurred during the charging process.

Table 3
Experiment data for different charging protocols.

Charging C-rate	Total charging time (s)	Coulomb efficiency (%)	Charge capacity (Ah)	Discharge capacity (Ah)	Net discharge from T_B to T_C (Ah)
2 C	1249	93.42	1.8051	1.6864	0.0706
1 C	2605	92.69	1.8812	1.7437	0.0913
0.5 C	5718	94.54	2.0655	1.9527	0.0459
1 C step-charging	5206	95.13	2.2225	2.1143	0
2 C step-charging	3570	99.72	2.2213	2.215	0

First, Table 3 indicates that the step-charging approach prevents lithium plating while achieving higher charging capacity and Coulomb efficiency, though it seemingly requires a longer total charging time. Fig. 11 illustrates the validation of the absence of a stripping signal in the dV/dQ curves during the subsequent discharging process when both types of step-charging are applied. Second, in terms of total charging time, the 1 C step-charging strategy analogously functions at an average current of about

0.53 C, closely resembling the 0.5 C protocol. Thus, when comparing the conventional 0.5 C charging with the 1 C step-charging, the latter not only prevents lithium plating but also results in a shorter total charging time, a greater total charge, and improved Coulomb efficiency. Third, similarly, the 2 C step-charging functions equivalently to a conventional CC charging at 0.77 C, effectively eliminating the risk of lithium deposition while enhancing Coulombic efficiency. Fourth, among all the tested protocols, the 2 C step-charging achieves the highest Coulombic efficiency, reaching 99.72% at 0 °C. This demonstrates its effectiveness as a charging strategy while completely avoiding lithium deposition risks.

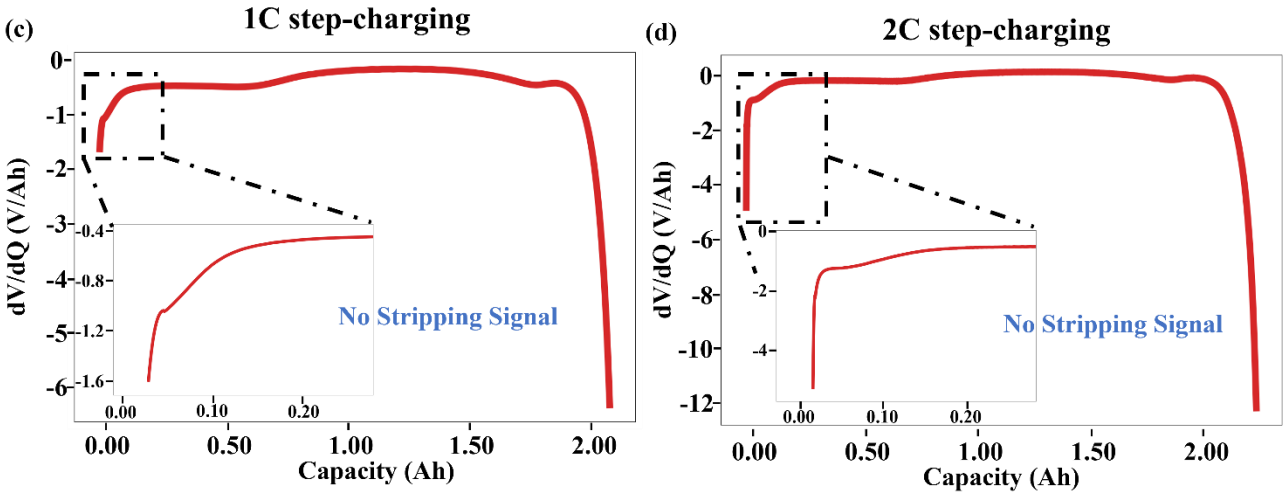

Fig. 11. The dV/dQ curves during discharge for (a) 1 C step-charging or (b) 2 C step-charging, where no striping signal is observed.

4.7. Discussions

Two aspects require further clarification: the extrapolated interpretations of data messages and the determination of the β ratio.

Linear fitting—The linear fitting technique employed in constructing the pseudo-P curve appears plausible, as the corresponding P curve in simulations demonstrates approximately linear behavior and can be regarded as a small current perturbation from its zero point. Confidence in the applicability of the linear extrapolation is supported by both the experiment in Sect. 4.2 and the simulation in Sect. 4.3.

β ratio—It is given as the net discharge capacity between T_B and T_C divided by the amount of lithium stripped during the same interval. With the reaction rate constant of the plating reaction set to $k_{pl} = 5.5 \times 10^{-8}$ m/s in our simulation [50], the β ratio is observed to be approximately 11.94% under 1 C charging across various cutoff voltages. Subsequent simulations reveal that the β ratio increases to around 23.30% at 0.5 C and decreases to approximately 7.22% at 2 C charging. Further simulation analysis confirms that variations in the k_{pl} give rise to different β values; however, the fundamental conclusions outlined above remain unaffected. Although the β ratio may vary, the different pseudo-P curves consistently intersect with the P curve at the same lithium-plating onset point at time T_A. This is due to the fact that the occurrence of lithium deposition is governed by the overpotential before plating, whereas β becomes relevant only after plating begins. This same intersection validates the robustness and utility of the pseudo-P curve approach. If the experimental β ratio is obtained, the total lithium plating can be estimated from the net discharge capacity, offering valuable insight for future studies on lithium deposition.

5. Conclusion

Monitoring lithium plating in commercial LIBs without disassembly is essential for risk management and safety evaluation during operation. This study introduces a pseudo-P curve approach to estimate the onset of lithium plating, relying solely on the signal acquired from a full-cell measurement. Based on the electrochemical simulation outcomes showing a consistent β ratio between the net discharge amount and the lithium stripping during discharging (equivalent to the lithium plating during charging when only reversible plating is taken into account) at the same C-rate, we construct a pseudo-P curve that intersects with the plating current curve (P curve). This intersection point marks the precise moment when lithium plating begins. The construction process requires: (i) measuring the net discharge capacity experimentally by identifying the valley point on the dV/dQ

discharge curve, and (ii) systematically varying the charging cutoff voltages to obtain multiple data points for linear fitting of the pseudo-P curve. The onset of lithium plating can still be predicted without requiring the exact value of the β ratio.

The PyBaMM simulation confirms the feasibility of the proposed pseudo-P curve approach. Moreover, its validity is also experimentally verified—without opening or compromising the battery's structural integrity—by detecting the presence or absence of stripping signals during discharging in cases where charging duration is either below or above the onset of lithium plating. Based on the identified onset moments across various charging C-rates, two step-charging protocols that completely avoid lithium plating are developed, with the 2 C step-charging protocol showing superior performance by achieving a Coulombic efficiency of 99.72% at 0 °C.

This study is still limited to the scenarios of fresh batteries at 0 °C. As LIBs age, it is expected that, under a fixed large charging C-rate, lithium plating of aged LIBs will occur earlier than that of fresh LIBs. This is attributed to the fact that increased impedance (characteristic of aged batteries) will inhibit lithium intercalation into the negative electrode. Lower environmental temperatures slow down reaction kinetics, also hindering lithium-ion transport and promoting the onset of lithium plating. A more comprehensive study on these topics, particularly gathering additional data to identify the onset points, will be essential for the future development of optimal charging strategies.

Acknowledgment

This work was supported by the National Science and Technology Council R.O.C. under Grant NSTC 112-2221-E-002-253-MY3.

References

[1] A. Tomaszewska, Z. Chu, X. Feng, S. O'Kane, X. Liu, J. Chen, M. Weng, Lithium-ion battery fast charging: A review, Etransportation 1 (2019) 100011. https://doi.org/10.1016/j.etran.2019.100011.

[2] J. Fan, S. Tan, Studies on charging lithium-ion cells at low temperatures, J. Electrochem. Soc. 153 (2006) A1081–A1086. https://doi.org/10.1149/1.2190029.

[3] T. Waldmann, B.-I. Hogg, M. Kasper, S. Grolleau, C. Gutiérrez Couceiro, K. Trad, B. P. Matadi, M. Wohlfahrt-Mehrens, Interplay of operational parameters on lithium deposition in lithium-ion cells: Systematic measurements with reconstructed 3-electrode pouch full cells, J. Electrochem. Soc. 163 (2016) A1232–A1239. https://doi.org/10.1149/2.0591607jes.

[4] M. Ecker, P. Shafiei Sabet, D.U. Sauer, Influence of operational condition on lithium plating for commercial lithium-ion batteries – Electrochemical experiments and post-mortem-analysis, Appl. Energy 206 (2017) 934–946. https://doi.org/10.1016/j.apenergy.2017.08.034.

[5] T. Waldmann, B.-I. Hogg, M. Wohlfahrt-Mehrens, Li plating as an unwanted side reaction in commercial Li-ion cells – A review, J. Power Sources 384 (2018) 107–124. https://doi.org/10.1016/j.jpowsour.2018.02.063.

[6] Y. Takagishi, T. Yamaue, Mathematical modeling of multiple-Li-dendrite growth in Li-ion battery electrodes, J. Electrochem. Soc. 170 (2023) 030528. https://doi.org/10.1149/1945-7111/acc2eb.

[7] N. Somasundaran, N. F. Saniee, T. Q. Dinh, J. Marco, Study on the extensibility of voltage-plateau-based lithium plating detection for electric vehicles, Energies 16 (2023) 2537. https://doi.org/10.3390/en16062537.

[8] U. Janakiraman, T.R. Garrick, M.E. Fortier, Review—Lithium plating detection methods in Li-ion batteries, J. Electrochem. Soc. 167 (2020) 160552. https://doi.org/10.1149/1945-7111/abd3b8.

[9] X. Lin, K. Khosravinia, X. Hu, J. Li, W. Lu, Lithium plating mechanism, detection, and mitigation in lithium-ion batteries, Prog. Energy Combust. Sci. 87 (2021) 100953. https://doi.org/10.1016/j.pecs.2021.100953.

[10] H. Zhou, C. Fear, R.E. Carter, C.T. Love, P.P. Mukherjee, Correlating lithium plating quantification with thermal safety characteristics of lithium-ion batteries, Energy Storage Mater. 66 (2024) 103214. https://doi.org/10.1016/j.ensm.2024.103214.

[11] M.-T. F. Rodrigues, K. Kalaga, S. E. Trask, D. W. Dees, I. A. Shkrob, D. P. Abraham, Fast charging of Li-ion cells: Part I. Using Li/Cu reference electrodes to probe individual electrode potentials, J. Electrochem. Soc. 166 (2019) A996. https://doi.org/10.1149/2.0401906jes.

[12] P. Kuntz, O. Raccurt, P. Azaïs, K. Richter, T. Waldmann, M. Wohlfahrt-Mehrens, S. Genies, Identification of degradation mechanisms by post-mortem analysis for high power and high energy commercial li-ion cells after electric vehicle aging, Batteries 7 (2021) 48. https://doi.org/10.3390/batteries7030048.

[13] C. Uhlmann, J. Illig, M. Ender, R. Schuster, E. Ivers-Tiffée, In situ detection of lithium metal plating on graphite in experimental cells, J. Power Sources 279 (2015) 428–438. https://doi.org/10.1016/j.jpowsour.2015.01.046.

[14] Y. Peng, M. Ding, K. Zhang, H. Zhang, Y. Hu, Y. Lin, Y. Yang, Quantitative Analysis of the Coupled Mechanisms of Lithium Plating, SEI Growth, and Electrolyte Decomposition in Fast Charging Battery, ACS Energy Lett. 9 (2024) 6022–6028. https://doi.org/10.1021/acsenergylett.4c02898.

[15] L. Xu, Y. Xiao, Y. Yang, R. Xu, Y.X. Yao, X.R. Chen, J.Q. Huang, In situ Li-plating diagnosis for fast-charging Li-ion batteries enabled by relaxation-time detection, Adv. Mater. 35 (2023) 2301881. https://doi.org/10.1002/adma.202301881.

[16] U.R. Koleti, T.Q. Dinh, J. Marco, A new on-line method for lithium plating detection in lithium-ion batteries, J. Power Sources 451 (2020) 227798. https://doi.org/10.1016/j.jpowsour.2020.227798.

[17] Y. Shen, X. Wang, Z. Jiang, B. Luo, D. Chen, X. Wei, H. Dai, Online detection of lithium plating onset during constant and multistage constant current fast charging for lithium-ion batteries, Appl. Energy 359 (2024) 123631. https://doi.org/10.1016/j.apenergy.2024.123631.

[18] Y. Chen, L. Torres-Castro, K.H. Chen, D. Penley, J. Lamb, M. Karulkar, N.P. Dasgupta, Operando detection of Li plating during fast charging of Li-ion batteries using incremental capacity analysis, J. Power Sources 539 (2022) 231601. https://doi.org/10.1016/j.jpowsour.2022.231601.

[19] J.G. Qu, Z.Y. Jiang, J.F. Zhang, Investigation on lithium-ion battery degradation induced by combined effect of current rate and operating temperature during fast charging, J. Energy Storage 52 (2022) 104811. https://doi.org/10.1016/j.est.2022.104811.

[20] M. Koseoglou, E. Tsioumas, D. Ferentinou, I. Panagiotidis, N. Jabbour, D. Papagiannis, C. Mademlis, Lithium plating detection using differential charging current analysis in lithium-ion batteries, J. Energy Storage 54 (2022) 105345. https://doi.org/10.1016/j.est.2022.105345.

[21] S. Schindler, M. Bauer, M. Petzl, M.A. Danzer, Voltage relaxation and impedance spectroscopy as in-operando methods for the detection of lithium plating on graphitic anodes in commercial lithium-ion cells, J. Power Sources 304 (2016) 170–180. https://doi.org/10.1016/j.jpowsour.2015.11.044.

[22] K. Sun, X. Li, Z. Zhang, X. Xiao, L. Gong, P. Tan, Pattern investigation and quantitative analysis of lithium plating under subzero operation of lithium-ion batteries, ACS Appl. Mater. Interfaces 15 (2023) 36356–36365. https://doi.org/10.1021/acsami.3c07098.

[23] F. Katzer, L. Jahn, M. Hahn, M.A. Danzer, Model-based lithium deposition detection method using differential voltage analysis, J. Power Sources 512 (2021) 230449. https://doi.org/10.1016/j.jpowsour.2021.230449.

[24] W. Huang, Y. Ye, H. Chen, R.A. Vilá, A. Xiang, H. Wang, Y. Cui, Onboard early detection and mitigation of lithium plating in fast-charging batteries, Nat. Commun. 13 (2022) 7091. https://doi.org/10.1038/s41467-022-33486-4.

[25] A. Mohammadi, S. Djafer, S. Sayegh, A.J. Naylor, M. Bechelany, R. Younesi, L. Stievano, Assessing coulombic efficiency in lithium metal anodes, Chem. Mater. 35 (2023) 2381–2393. https://doi.org/10.1021/acs.chemmater.2c03518.

[26] M. Koseoglou, E. Tsioumas, D. Ferentinou, N. Jabbour, D. Papagiannis, C. Mademlis, Lithium plating detection using dynamic electrochemical impedance spectroscopy in lithium-ion batteries, J. Power Sources 512 (2021) 30508. https://doi.org/10.1016/j.jpowsour.2021.230508.

[27] S. Ding, Y. Li, H. Dai, L. Wang, X. He, Accurate model parameter identification to boost precise aging prediction of lithium-ion batteries: A review, Adv. Energy Mater. 13 (2023) 2301452. https://doi.org/10.1002/aenm.202301452.

[28] J. Li, L. Wang, J. Xu, Investigation of the lithium plating triggering criterion in graphite electrodes, J. Mater. Chem. A 12 (2024) 12581–12591. https://doi.org/10.1039/D4TA00244J.

[29] X. Duan, B. Li, J. Li, X. Gao, L. Wang, J. Xu, Quantitative understanding of lithium deposition-stripping process on graphite anodes of lithium-ion batteries, Adv. Energy Mater. 13 (2023) 2203767. https://doi.org/10.1002/aenm.202203767.

[30] T. Sun, T. Shen, Y. Zheng, D. Ren, W. Zhu, J. Li, Y. Wang, K. Kuang, X. Rui, S. Wang, L. Wang, X. Han, L. Lu, M. Ouyang, Modeling the inhomogeneous lithium plating in lithium-ion batteries induced by non-uniform temperature distribution, Electrochim. Acta 435 (2022) 140701. https://doi.org/10.1016/j.electacta.2022.140701.

[31] P. Arora, M. Doyle, R.E. White, Mathematical modeling of the lithium deposition overcharge reaction in lithium-ion batteries using carbon-based negative electrodes, J. Electrochem. Soc. 146 (1999) 3543. https://doi.org/10.1149/1.1392512.

[32] S. Wang, D. Ren, C. Xu, X. Han, X. Liu, L. Lu, M. Ouyang, Lithium plating induced volume expansion overshoot of lithium-ion batteries: Experimental analysis and modeling, J. Power Sources 573 (2023) 233946. https://doi.org/10.1016/j.jpowsour.2023.233946.

[33] H. Wang, Y. Song, X. Sun, S. Mo, C. Chen, J. Wang, Onboard in-situ warning and detection of Li plating for fast-charging batteries with deep learning, Energy Storage Mater. 71 (2024) 103585. https://doi.org/10.1016/j.ensm.2024.103585.

[34] R. Mathieu, O. Briat, P. Gyan, J.-M. Vinassa, Fast charging for electric vehicles applications: Numerical optimization of a multi-stage charging protocol for lithium-ion battery and impact on cycle life, J. Energy Storage 40 (2021) 102756. https://doi.org/10.1016/j.est.2021.102756.

[35] H.E. Ouazzani, I.E. Hassani, N. Barka, T. Masrour, MSCC-DRL: Multi-Stage constant current based on deep reinforcement learning for fast charging of lithium ion battery, J. Energy Storage 75 (2024) 109695. https://doi.org/10.1016/j.est.2023.109695.

[36] D. Ji, L. Chen, T. Ma, J. Wang, S. Liu, X. Ma, F. Wang, Research on adaptability of charging strategy for electric vehicle power battery, J. Power Sources 437 (2019) 226911. https://doi.org/10.1016/j.jpowsour.2019.226911.

[37] M. Dotoli, E. Milo, M. Giuliano, A. Tiozzo, M. Baricco, C. Nervi, M. Ercole, M.F. Sgroi, Development of an innovative procedure for lithium plating limitation and characterization of 18650 cycle aged cells for DCFC automotive applications, Batteries 8 (2022) 88. https://doi.org/10.3390/batteries8080088.

[38] Q. Liu, C. Du, B. Shen, P. Zuo, X. Cheng, Y. Ma, G. Yin, Y. Gao, Understanding undesirable anode lithium plating issues in lithium-ion batteries, RSC Adv. 6 (2016) 88683–88700. https://doi.org/10.1039/C6RA19482F.

[39] H. Ge, T. Aoki, N. Ikeda, S. Suga, T. Isobe, Z. Li, Y. Tabuchi, J. Zhang, Investigating lithium plating in lithium-ion batteries at low temperatures using electrochemical model with NMR assisted parameterization, J. Electrochem. Soc. 164 (2017) A1326–A1334. https://doi.org/10.1149/2.0461706jes

[40] D. Ren, K. Smith, D. Guo, X. Han, X. Feng, L. Lu, M. Ouyang, J. Li, Investigation of lithium plating-stripping process in Li-ion batteries at low temperature using an electrochemical model, J. Electrochem. Soc. 165 (2018) A2167. https://doi.org/10.1149/2.0661810jes.

[41] X.-G. Yang, S. Ge, T. Liu, Y. Leng, C.-Y. Wang, A look into the voltage plateau signal for detection and quantification of lithium plating in lithium-ion cells, J. Power Sources 395 (2018) 251–261. https://doi.org/10.1016/j.jpowsour.2018.05.073.

[42] S.E.J. O'Kane, I.D. Campbell, M.W.J. Marzook, G.J. Offer, M. Marinescu, Physical origin of the differential voltage minimum associated with lithium plating in Li-ion batteries, J. Electrochem. Soc. 167 (2020) 090540. https://doi.org/10.1149/1945-7111/ab90ac.

[43] N. Legrand, B. Knosp, P. Desprez, F. Lapicque, S. Raël, Physical characterization of the charging process of a Li-ion battery and prediction of Li plating by electrochemical modelling, J. Power Sources 245 (2014) 208–216. https://doi.org/10.1016/j.jpowsour.2013.06.130.

[44] M. Petzl, M.A. Danzer, Nondestructive detection, characterization, and quantification of lithium plating in commercial lithium-ion batteries, J. Power Sources 254 (2014) 80–87. https://doi.org/10.1016/j.jpowsour.2013.12.060.

[45] W. Mei, Y. Zhang, Y. Li, P. Zhuo, Y. Chu, Y. Chen, L. Jiang, H. Zhou, J. Sun, Q. Wang, Unveiling voltage evolution during Li plating-relaxation-Li stripping cycling of lithium-ion batteries, Energy Storage Mater. 72 (2024) 103193. https://doi.org/10.1016/j.ensm.2024.103193.

[46] V. Sulzer, S.G. Marquis, R. Timms, M. Robinson, S.J. Chapman, Python battery mathematical modelling (PyBaMM), J. Open Res. Softw. 9 (2021). https://doi.org/10.5334/jors.309.

[47] N. Collath, H. Winner, A. Frank, A. Durdel, A. Jossen, Suitability of late-life lithium-ion cells for battery energy storage systems, J. Energy Storage 87 (2024) 111508. https://doi.org/10.1016/j.est.2024.111508.

[48] L. Jin, M. Kazemi, G. Comodi, C. Papadimitriou, Assessing battery degradation as a key performance indicator for multi-objective optimization of multi-carrier energy systems, Appl. Energy 361 (2024) 122925. https://doi.org/10.1016/j.apenergy.2024.122925.

[49] C.H. Chen, F. Brosa Planella, K. O'Regan, D. Gastol, W.D. Widanage, E. Kendrick, Development of experimental techniques for parameterization of multi-scale lithium-ion battery models, J. Electrochem. Soc. 167 (2020) 080534. https://doi.org/10.1149/1945-7111/ab9050.

[50] S.E.J. O'Kane, W. Ai, G. Madabattula, D. Alonso-Alvarez, R. Timms, V. Sulzer, J.S. Edge, B. Wu, G.J. Offer, M. Marinescu, Lithium-ion battery degradation: how to model it, Phys. Chem. Chem. Phys. 24 (2022) 7909–7922. https://doi.org/10.1039/D2CP00417H.

[51] P. Brodsky Ringler, M. Wise, P. Ramesh, J.H. Kim, M. Canova, C. Bae, J. Deng, H. Park, Modeling of lithium plating and stripping dynamics during fast charging, Batteries 9 (2023) 337. https://doi.org/10.3390/batteries9070337.

[52] V. Sulzer, P. Mohtat, S. Pannala, J.B. Siegel, A.G. Stefanopoulou, Accelerated battery lifetime simulations using adaptive inter-cycle extrapolation algorithm, J. Electrochem. Soc. 168 (2021) 120531. https://doi.org/10.1149/1945-7111/ac3e48.

[53] J.H. Yang, K.C. Chen, Evaluation of electrochemical parameters for cycle aging $LiCoO_2$ lithium-ion batteries by quantifying the incremental capacity curve, J. Electrochem. Soc. 169 (2022) 020517. https://doi.org/10.1149/1945-7111/ac4db2.

[54] J. Hong, F. Liang, Y. Chen, F. Wang, X. Zhang, K. Li, H. Zhang, J. Yang, C. Zhang, H. Yang, S. Ma, Q. Yang, A novel battery abnormality diagnosis method using multi-scale normalized coefficient of variation in real-world vehicles, Energy 297 (2024) 131475. https://doi.org/10.1016/j.energy.2024.131475.

[55] J. Luo, K. Ying, P. He, J. Bai, Properties of Savitzky–Golay digital differentiators, Digit. Signal Process. 15 (2005) 122–136. https://doi.org/10.1016/j.dsp.2004.09.008.

[56] Y. Yuan, H. Wang, X. Han, Y. Pan, Y. Sun, X. Kong, L. Lu, M. Ouyang, The local lithium plating caused by anode crack defect in Li-ion battery, Appl. Energy 361 (2024) 122968. https://doi.org/10.1016/j.apenergy.2024.122968.

[57] W. Mei, L. Zhang, J. Sun, Q. Wang, Experimental and numerical methods to investigate the overcharge caused lithium plating for lithium ion battery, Energy Storage Mater. 32 (2020) 91–104. https://doi.org/10.1016/j.ensm.2020.06.021.

[58] R. Bednorz, T. Gewald, Investigation of the effects of charging processes on lithium-ion cells with SiC anodes at low temperatures, Batteries 6 (2020) 34. https://doi.org/10.3390/batteries6020034.

[59] T. Waldmann, M. Kasper, M. Wohlfahrt-Mehrens, Optimization of charging strategy by prevention of lithium deposition on anodes in high-energy lithium-ion batteries - Electrochemical experiments, Electrochim. Acta 178 (2015) 525–532. https://doi.org/10.1016/j.electacta.2015.08.056.